

# Neural Ordinary Differential Equation Control of Dynamics on Graphs

Thomas Asikis<sup>1</sup>, Lucas Böttcher<sup>2</sup>, and Nino Antulov-Fantulin<sup>1</sup>

<sup>1</sup>ETH Zürich, Switzerland

<sup>2</sup>UCLA, Los Angeles, USA

<sup>1</sup>{*asikist, anino*}@ethz.ch

<sup>2</sup>*lucasb@g.ucla.edu*

August 16, 2021

## Abstract

We study the ability of neural networks to steer or control trajectories of continuous time non-linear dynamical systems on graphs, which we represent with neural ordinary differential equations (neural ODEs). To do so, we introduce a neural-ODE control (NODEC) framework and find that it can learn control signals that drive graph dynamical systems into desired target states. While we use loss functions that do not constrain the control energy, our results show that NODEC produces low energy control signals. Finally, we showcase the performance and versatility of NODEC by using it to control a system of more than one thousand coupled, non-linear ODEs.

## 1 Introduction

Dynamical processes on complex networks are common tools to model a wide range of real-world phenomena including opinion dynamics [21, 43], epidemic spreading [23, 4, 19], synchronization [77, 97], and financial distress propagation [31]. Continuous-time dynamics on complex networks can be described by different frameworks including Chapman–Kolmogorov [92], Fokker–Planck [68], stochastic differential [3], and ordinary differential [26, 39, 11] equations. The structure of many

real-world systems is described by networks with certain common properties including small-world effects [93], heavy-tail degree distributions [76, 9], community structure [38], and other features [33, 54]. The control of dynamical processes on networks [59, 58] is a challenging task with applications in engineering, biology, and the social sciences [10, 73]. Control signals can be calculated by solving boundary-value PMP problems [63, 48, 65], or computing solutions of the Hamilton–Jacobi–Bellman equation (HJB). Complementing the above approaches, we develop a Neural-ODE control (NODEC) framework that controls fully observable graph dynamical systems using neural ODEs [27]. Within this framework, feedback control signals are calculated by minimizing a loss functional describing differences between the current and target states. We perform extensive numerical experiments on coupled high-dimensional non-linear dynamical systems to showcase the ability of NODEC to calculate effective control signals.

Mathematically, systems are “controllable” if they can be steered from any initial state  $\mathbf{x}(t_0)$  to any desired state  $\mathbf{x}^*(T)$  in finite time  $T$ . For linear systems, an analytical condition for controllability of linear time-invariant (LTI) systems was derived by Kalman in the 1960s [47] and is known today as Kalman’s rank criterion. In 1969, Popov, Belevitch, and Hautus [42] introduced another controllability test for LTI systems that relies on solutions of an

eigenvalue problem of the state matrix. In the 1970s, Lin introduced the framework of structural controllability [56] as a generalization of prior definitions of controllability on graphs. More recently, different large-scale social, technical, and biological networks were analyzed from a network controllability perspective [59, 78] building on the framework introduced by Lin [56]. Controlling a complex system becomes more challenging as the number of nodes that can receive a control signal (driver nodes) decreases. Furthermore, Ref. [96] addresses the important issue of quantifying the (control) energy that is needed to control LTI systems. Steering the dynamical system to the target state becomes even harder when energy minimization is also accounted for.

To solve general non-linear optimal control problems with energy and driver node constraints, two main approaches are used: (i) Pontryagin’s maximum principle (PMP) [63, 48, 65] and (ii) Bellman’s (approximate) dynamic programming [100, 34, 13, 90, 52]. Pontryagin’s maximum principle [63, 48, 65] is based on variational calculus and transforms the original infinite-dimensional control problem to a boundary-value problem in a Hamiltonian framework. The downside of this approach is that the resulting boundary-value problems are often very difficult to solve. An alternative to variational methods is provided by Bellman’s dynamic programming, which relies on the HJB equation. Given a quadratic loss on the control input, the HJB equation can be transformed into a partial-differential equation (PDE) [34]. Dynamic programming and PMP are connected through the viscosity solutions of the aforementioned PDEs [100]. However, in most cases, the HJB equation is hard to solve [13] and does not admit smooth solutions [35]. Most reinforcement-learning-based controls [90] rely on optimizing the HJB equation and can be viewed as an approximation of the dynamic programming [52] approach.

In this article we propose an alternative approach, where we extend the neural ordinary differential equation framework to solve control problems. We describe and evaluate the ability of neural ordinary differential equation control (NODEC) to efficiently control non-linear continuous time dynamical systems by calculating feedback control signals. In section 2, we discuss related work. Section 3 summarizes mathematical concepts that are relevant for controlling graph dynamical systems. In section 4, we provide an overview of the basic features of NODEC and

formulate conditions for its successful application to solve control problems. In section 5, we showcase the ability of NODEC to efficiently control different graph dynamical systems that are described by coupled ODEs. In particular, we use NODEC to calculate feedback controls that synchronize coupled oscillators and contain disease dynamics with limited number of driver nodes. Interestingly, NODEC achieves low energy controls without sacrificing performance. Section 6 concludes our paper.

## 2 Related Work

Previous works used neural networks in control applications [55], in particular for parameter estimation of model predictive control [98, 2]. Extensive applications of neural networks are also found in the field of Proportional-Integral-Derivative (PID) controllers [55], where the gain factors are calculated via neural networks. Shallow neural networks have been trained to interact with and control smaller-scale ODE systems [55], without using neural ODEs or deep architectures. Recently, deep neural networks have demonstrated high performance in control tasks, and notably on related work on differentiable physics [44] that often use PMP. Deep reinforcement learning [72] models are also used and rely on approximation of the HJB approach. Other gradient-based non-neural network approaches rely on the usage of adjoint methods [17]. Such model approaches follow the solutions of the PMP principle and calculus of variations solutions. One can also design generic approaches to control network dynamics [94, 29]. Optimal control with NODEC, where the input of the neural network is only the time variable  $t$  is extensively studied in Ref. [20], where it is compared with analytically derived methods. The current work focuses on feedback control methods on non-linear dynamical systems, where minimum energy controls are not always known. In our work, we always choose state-of-the-art control solutions when available, such as feedback control [86] and deep reinforcement learning methods [40, 36], so that we can compare NODEC performance with corresponding baselines. The main contributions of this work are: (i) introduction of an adaptive efficient feedback control approximation methodology with implicit energy regularization properties that relies on neural ODEs, (ii) detailed numerical experiments involving high-dimensional non-linear

dynamical systems with minimum driver node constraints, and (iii) an extensively tested codebase that can be easily used and extended on other nonlinear control applications.

### 3 Feedback Control of Graph Dynamical Systems

A graph  $G(V, E)$  is an ordered pair, where  $V$  and  $E \subseteq V \times V$  are the corresponding sets of  $|V| = N$  nodes and edges. Although, in network science [69], it is more common to refer to graphs as networks, in this paper we will use the term “graph” instead of “network” to avoid confusion with neural networks.

Throughout this paper, we study dynamical systems on graphs described by the adjacency-matrix  $\mathcal{A}$ , which has non-zero elements  $\mathcal{A}_{ij}$  if and only if nodes  $i$  and  $j$  are connected. We describe controlled graph dynamical systems by ODEs of the form

$$\dot{\mathbf{x}}(t) = f(\mathbf{x}(t), \mathcal{A}, \mathbf{u}(\mathbf{x}(t))), \quad (1)$$

where  $\mathbf{x}(t) \in \mathbb{R}^N$  denotes the state vector and  $\mathbf{u}(t) \in \mathbb{R}^M$  ( $M \leq N$ ) an external control. We use Newton’s dot notation for differentiation  $\dot{\mathbf{x}}(t)$ . The function  $f$  in Equation (1) accounts for both (time-dependent) interactions between nodes and the influence of external control signals on the evolution of  $\mathbf{x}(t)$ . We assume that the system state  $\mathbf{x}$  is fully observable. In control theory, the control signal  $u(t)$  is often calculated via two approaches: either by using time as input (i.e.,  $\mathbf{u} = \mathbf{u}(t)$ ) [96] or by using the system’s state at time  $t$  as input (i.e.,  $\mathbf{u} = \mathbf{u}(\mathbf{x}(t))$ ) [64]. The latter calculation is often used in state-feedback control [64], where the control signal is calculated as a function of the difference between the current system target state and the control target state  $g(\mathbf{x}(t) - \mathbf{x}^*)$ . In the present article, we focus on state-feedback control and denote control signals by  $\mathbf{u}(\mathbf{x}(t))$ . The applicability of the current framework on time-dependent controls is evaluated in detail in Ref. [20].

In principle, eq. (1) can be solved numerically, for instance using an explicit Euler scheme: For some given state  $\mathbf{x}(t)$  at time  $t$ , the state of the system at time  $t + \Delta t$  is  $\mathbf{x}(t + \Delta t) = \mathbf{x}(t) + \Delta t f(\mathbf{x}(t), \mathbf{u}(\mathbf{x}(t)))$ . Apart from an Euler forward integration scheme, there exist many more numerical methods [84] to solve eq. (1). We use the expression `ODESolve( $\mathbf{x}(t), t, T, f, \mathbf{u}(\mathbf{x}(t))$ )` to indicate a generic ODE

solver that uses the right-hand side of eq. (1) as an input and computes  $\mathbf{x}(T)$  for a given  $\mathbf{x}(t)$  if  $T > t$ . In section 5, we employ Dormand–Prince and Runge–Kutta schemes as our ODEsolve methods. Nevertheless, when numerically calculating analytical solutions may introduce numerical instabilities and can be computationally expensive for large systems. Numerical methods are also required for general non-linear ODE systems, which do not have analytic tractable solutions of optimal control signals. Additionally, as mentioned in section 1, the control of a complex dynamical system becomes more challenging when considering minimum energy and driver node constraints.

#### 3.1 Driver Node Selection

Our aim is to showcase the ability of NODEC to produce efficient feedback controls for systems where the number driver nodes approaches the minimum number necessary to achieve control. Thus, we need to identify set of driver nodes that are able to fully control the underlying dynamics. Usually, we are interested in finding the minimum set of driver nodes, which is equivalent to the graph-theoretical problems of maximum matching or minimum edge dominating sets [28, 95]. However, for general graphs, finding the maximum matching set is NP-hard [37, 70]. In our NODEC framework, we determine driver nodes according to two methods: (i) the maximum matching method [59] for disease dynamics and (ii) from stability criteria in the case of Kuramoto oscillators [85]. We denote the set of driver nodes and its cardinality by  $\mathbb{B} \subseteq V$  and  $M$ , respectively. A driver matrix  $B \in \mathbb{R}^{N \times M}$ , where we set  $B_{ij} = 1$  if  $i \in \mathbb{B}$  and  $u_j$  is applied on  $i$  and  $B_{ij} = 0$  otherwise. Although the literature is rich in studies on driver node placement on graphs, there is considerably fewer work that addresses ways of efficiently finding control inputs for high-dimensional dynamical systems with a limited number of driver nodes.

#### 3.2 Control Energy Constraints

In complex systems, it may not always be possible to apply any control signal to a driver node. Consider a disease that spreads between networked communities (nodes) and a control signal that denotes the intensity of quarantine. Applying a constant control signal with high values indicating blanket lockdown measures may not be acceptable

by society. In the given example, our goal would be to contain disease spreading as much as possible, while applying appropriate control signals to the driver nodes. A widely used metric for the intensity of the control signal [59] is the control energy

$$\mathcal{E}[\mathbf{u}(T)] = \int_0^T \|\mathbf{u}(t)\|_2^2 dt, \quad (2)$$

where  $\|\cdot\|_2$  denotes the L2 norm. In our numerical experiments eq. (2), we approximate the corresponding integral by

$$\mathcal{E}[T] \approx \sum_{k=1}^K \|\mathbf{u}(t_0 + k\Delta t)\|_2^2 \Delta t, \quad (3)$$

In Ref. [20], we show that NODEC approximates optimal (or minimum energy) control signals without the necessity of explicitly accounting for an integrated energy cost in the underlying loss function. Instead, NODEC implicitly minimizes the control energy via the interplay of an induced gradient descent, neural-ODE solver dynamics, and neural-network initialization. Avoiding the control energy term in a constrained optimization also reduces computational cost of learning compared to solving boundary-value PMP problems [63, 48, 65], or computing solutions of the Hamilton–Jacobi–Bellman equation (HJB) equation [100, 34, 13, 90, 52]. In the present article, we provide evidence that NODEC achieves lower energy and higher performance when compared to feedback controls for large complex systems.

## 4 Neural ODE Control

As in section 3, we consider a dynamical system (1) with initial state  $\mathbf{x}(t_0)$ , reached state  $\mathbf{x}(t)$ , and target state  $\mathbf{x}^*$ . The goal of NODEC is to minimize differences between  $\mathbf{x}(t)$  and  $\mathbf{x}^*$  using control inputs  $\hat{\mathbf{u}}(\mathbf{x}, t; \mathbf{w})$ , where the vector  $\mathbf{w}$  represents the weights of an underlying neural network. We quantify differences between reached and target states with the loss function  $J(\mathbf{x}(T), \mathbf{x}^*; \mathbf{w})$ . The general NODEC procedure is thus based on finding weights  $\mathbf{w}$  that minimize  $J(\mathbf{x}(T), \mathbf{x}^*; \mathbf{w})$  under the constraint (1), using a gradient descent update rule over a certain number of epochs. That is,

$$\begin{aligned} & \min_{\mathbf{w}} J(\mathbf{x}(T), \mathbf{x}^*; \mathbf{w}) \\ & \text{s.t. } \dot{\mathbf{x}}(t) = f(t, \mathbf{x}(t), \mathbf{u}(t)), \end{aligned} \quad (4)$$

where  $\mathbf{u}(t) = \hat{\mathbf{u}}(\mathbf{x}, t; \mathbf{w})$  and

$$\mathbf{w} \leftarrow \mathbf{w} + \Delta \mathbf{w} \quad \text{with} \quad \Delta \mathbf{w} = -\eta \nabla_{\mathbf{w}} J(\mathbf{x}(T), \mathbf{x}^*; \mathbf{w}). \quad (5)$$

Our proposed method relies on the usage of neural ODEs [27], which are a natural choice for the approximation of continuous-time control signals. Using neural ODEs instead of discrete-time controls allows us to approximate a continuous-time interaction and express the control function  $\hat{\mathbf{u}}(\mathbf{x}, t; \mathbf{w})$  as a parameterized neural network within an ODE solver (fig. 1).

The NODEC framework can be used to control both linear and non-linear graph dynamical systems with various loss functions. Our approach is of particular relevance for continuous time control problems with unknown and intractable optimal control functions. NODEC is based on universal approximation theorems for the approximation of continuous-time control functions with neural networks (NNs) and able to learn control inputs directly from the dynamics in an interactive manner akin to Reinforcement Learning (RL). Contrary to other control approaches [96, 34, 63, 48, 65], we do not impose a control energy constraint directly on our optimization loss function, improving the learning efficiency considerably.<sup>1</sup>

In Algorithms 1 and 2, we show the two parts of a generic NODEC algorithm that approximates control signals. The main elements of NODEC are: (i) input and target states, (ii) graph coupled dynamics, (iii) neural network architecture and initialization, the parameters of the (iv) ODE solver (e.g., step-size) and of the (v) gradient descent algorithm and its hyper-parameters, such as learning rate. Note that Algorithm 2 relies on the automatic differentiation methods [12, 74], where the gradients “flow” through the underlying neural network, that is time-unfolded by ODE solvers [84].

### 4.1 Neural ODE and NODEC Learning Settings

Although NODEC utilizes neural ODEs [27], the learning tasks of both frameworks differ significantly. Neural

<sup>1</sup>Imposing an energy constraint would require collecting and back-propagating the norm of all control inputs at each time step during training. Using such a back-propagation scheme would increase training times considerably because of the potentially large number of control inputs in large-scale graph dynamical systems.

---

**Algorithm 1:** A generic algorithm that describes the parameter learning of NODEC.

---

```

Result:  $\mathbf{w}$ 
1 Init:  $\mathbf{x}_0, \mathbf{w}, f(\cdot), \text{ODESolve}(\cdot), J(\cdot), \mathbf{x}^*$ ;
2 Params:  $\eta$ , epochs;
3 epoch  $\leftarrow 0$ ;
4 while epoch < epochs do
5    $t \leftarrow 0$ ;
6    $\mathbf{x} \leftarrow \mathbf{x}_0$ ;
7   // Generate a trajectory based on NODEC.
   $\mathbf{x} \leftarrow \text{ODESolve}(\mathbf{x}, 0, T, f, \hat{\mathbf{u}}(\mathbf{x}, t; \mathbf{w}))$ ;
8   // gradient descent update
   $\mathbf{w} \leftarrow \mathbf{w} - \eta \nabla_{\mathbf{w}} J(\mathbf{x}, \mathbf{x}^*)$ ;
9   // or Quasi-Newton with Hessian:
  //  $\mathbf{w} \leftarrow \mathbf{w} - \eta H^{-1} \nabla_{\mathbf{w}} J(\mathbf{x}, \mathbf{x}^*)$ 
10 end

```

---

**Algorithm 2:** A simple ODESolve implementation.

---

```

1 Function  $\text{ODESolve}(\mathbf{x}, t, T, f, \hat{\mathbf{u}}(\mathbf{x}, t; \mathbf{w}))$ :
  // Euler Method
2 while  $t \leq T$  do
  // Computational graph is
  // preserved through time
  // gradients flow through  $\mathbf{x}$ 
3    $\hat{\mathbf{u}} \leftarrow \hat{\mathbf{u}}(\mathbf{x}, t; \mathbf{w})$ ;
4    $\mathbf{x} \leftarrow \mathbf{x} + \tau f(\mathbf{x}, \hat{\mathbf{u}})$ ;
  // Step  $\tau$  could be adaptive
5    $t \leftarrow t + \tau(t)$ ;
6 end
7 return  $\mathbf{x}$ ;
8 end

```

---

ODEs [27] model dynamics of the hidden state of a neural network according to

$$\dot{\mathbf{h}}(t) = f(t, \mathbf{h}(t), \mathbf{w}), \quad (6)$$

where  $f(\mathbf{h}(t), t, \mathbf{w})$  and  $\dot{\mathbf{h}}(t)$  represent the neural network and hidden-state derivative, respectively. Previously, neural ODEs were mainly applied in supervised learning tasks [50] and in normalizing flows [27]. For NODEC, we use a neural network as a parameterized function to approximate the control term  $\mathbf{u}(t)$  in graph dynamical systems (1). Contrary to supervised applications of neural ODEs [27], our proposed framework numerically solves control problems in an interactive manner, similar to reinforcement learning.

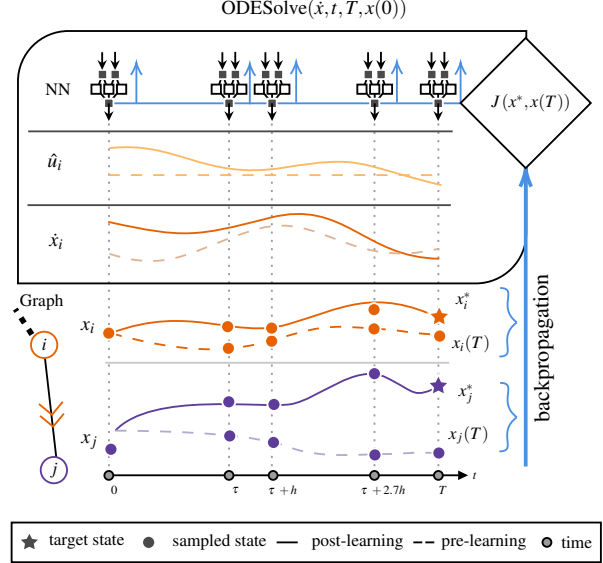


Figure 1: A schematic that summarizes the training process of NODEC. A NN learns the control within the ODESolver.

## 4.2 Learnability of Control with Neural Networks

As reachability of a target state  $\mathbf{x}^*$  from an initial state  $\mathbf{x}(t_0)$  implies the existence of a control function  $\mathbf{u}(t)$ , we now focus on the ability to approximate (i.e., learn)  $\mathbf{u}(\mathbf{x}(t))$  for reachable target states with a neural network.

**Proposition 1.** *Given that (i) a target state  $\mathbf{x}^*$  is reachable with continuous time dynamics (1) and (ii) the control function  $\mathbf{u}(t)$  is continuous or Lebesgue integrable in its domain, a neural network for which a corresponding universal approximation (UA) theorem applies can approximate a control function  $\hat{\mathbf{u}}(t; \mathbf{w}) \rightarrow \mathbf{u}(t)$  by learning parameters  $\mathbf{w}$ .*

The above propositions hold when an appropriate UA theorem [88, 99, 81, 87, 41] and reachability [60] requirements are satisfied by the underlying dynamics and the neural network controller. The ability of a neural network to learn control signals has also been covered in the literature outside of the domain of neural ODEs [24, 45, 98, 16]. In the current work we choose to compare our proposed model to an analytical feedback control baseline [85] and

state-of-the-art reinforcement learning [36] for non-linear dynamical systems describing for Kuramoto oscillators and disease spreading.

### 4.3 Learning Loss and Control Targets

To apply NODEC to control tasks, we have to translate a control goal into an adequate learning loss. The choice of the control goal depends on the underlying dynamics, graph structure, and objectives of the control designer. A very common goal in literature [57] is “microscopic” control where each node  $i$  has to reach a predetermined state value within time  $T$ , i.e.  $x_i(T) = x_i^*$ . Such a control target is common in industrial applications and may be used to steer electric and mechanical systems [57]. This goal is achieved by minimizing a metric that quantifies the distance between the target and reached states  $\mathbf{x}(T)$  and  $\mathbf{x}^*$ . One possible choice of such a metric is the mean squared error (MSE)  $J(\mathbf{x}(T), \mathbf{x}^*) = \frac{1}{N} \sum_{i=1}^N (x_i(T) - x_i^*)^2$ . When the MSE is used, corresponding optimal control problems may be expressed as convex optimization problems [14]. For more details on the application of NODEC to microscopic loss function, see Ref. [20].

We focus on control goals that do not require a specific target state value for each node, but instead require that constraints over aggregate values or statistical properties of the system’s states are satisfied. For the control of certain complex systems, it is useful to consider such “macroscopic” constraints [83, 10]. Often such goals lack exact optimal control solutions, thus offering many opportunities for novel control applications of NODEC. A common macroscopic control goal is that nodes in the target state are required to be synchronized, i.e. the nodes’ states are required to have the same value or constant phase shifts. Such synchronization conditions are often considered in the context of controlling oscillator systems [17, 22]. We also consider more complex control goals, when the system evolution includes coupled ODEs with more than one state variable, such as disease spreading dynamics. In the context of epidemic models, the state  $\mathbf{x}$  is represented by a matrix, that consists of multiple state variables. For susceptible-infected-recovered (SIR) models, three state variables,  $S_i(t)$ ,  $I_i(t)$ , and  $R_i(t)$ , are used to model the part of a population on node  $i$  at time  $t$  that is susceptible, infected, and recovered, respectively.

## 5 Experimental Evaluation

In this section, we evaluate the ability of NODEC to (i) reach target states efficiently with a limited number of driver nodes, (ii) control different dynamics and losses, and (iii) calculate low energy signals. We first evaluate the performance of NODEC for two non-linear systems with very different control tasks to showcase its applicability and versatility in computationally challenging settings for which analytical solutions or approximate control schemes may not exist. We describe the experimental setup by defining the dynamical systems, initial state, control goal, and neural-network hyperparameters used for training. The choice of neural-network hyperparameters focuses mainly on the network architecture, inputs, optimizers, and training procedures. For the sake of brevity, we omit technical details in the main text and provide further information in the Supplemental Material and in our code[6, 7] and data repositories[5].

### 5.1 Coupled Oscillator Dynamics

In this section, we study the ability of NODEC to control a network of coupled oscillators via feedback control. Such systems are used to model power grids and brain networks [30, 32]. One common control goal for oscillator systems is to reach a fully synchronized target state and stabilize the system over time. This introduces two main challenges: (i) a target state that satisfies this goal needs to be reached and preserved and (ii) the trained model needs to be able to achieve synchronization stability for initial states not seen in training. For CT-LTI systems and systems that can be linearized, there exist optimal feedback control methods [82]. Continuous-time oscillatory dynamics may not always be linearizable [85] and exhibit chaotic behavior [18, 62], which cannot be observed in (finite-dimensional) LTI systems. NODEC does not require linearization and could potentially control systems that are costly or intractable to linearize.

In a graph of  $N$  coupled oscillators, a possible mathematical description of the evolution of phase  $x_i$  of oscillator  $i$  with natural frequency  $\omega_i$  is

$$\dot{x}_i = \omega_i + B_i u_i(x(t)) + K \sum_j \mathcal{A}_{i,j} h(x_j - x_i) \quad (7)$$

where  $\mathcal{A}$  is the interaction matrix,  $K$  the coupling constant,

and  $h$  a  $2\pi$ -periodic function [85]. The driver matrix  $B$  connects control inputs  $\mathbf{u}(t)$  to the corresponding nodes. For  $2\pi$ -periodic oscillator dynamics (7), optimal feedback control can be achieved via linearization near the steady state [85] and are known to work only for low values of coupling frustration [85].

$$\mathbf{x}^\diamond = \Xi^{-1} L^\dagger \boldsymbol{\omega}, \quad (8)$$

where  $L^\dagger$  is the pseudoinverse of the graph Laplacian.

To study the performance of NODEC, we consider the Kuramoto model [53]

$$\dot{x}_i = \omega_i + B_{ii} u_i[x(t)] + \Xi \sum_j \mathcal{A}_{i,j} \sin(x_j - x_i) \quad (9)$$

as a specific example of a model of coupled oscillators in a network.

### 5.1.1 Control Baselines

A feedback control (FC) baseline for Kuramoto dynamics is presented in Ref. [85]. The control signals and driver matrix elements satisfy

$$\begin{aligned} u_i &= \zeta B_{i,i} \sin(x_i^* - x_i), \\ B_{i,i} &\geq \Xi \sum_{j \neq i} \mathcal{A}_{i,j} [|\cos(x_i^\diamond - x_j^\diamond)| - \cos(x_j^\diamond - x_i^\diamond) - \varepsilon]. \end{aligned} \quad (10)$$

Observe that  $B$  can only have diagonal elements with non-zero values, which can also be referred to as control gains. Driver nodes thus satisfy  $B_{i,i} \neq 0$ . An error margin buffer is also implemented as suggested in related work [85] by setting  $\varepsilon \geq 0$  when selecting driver nodes. For  $\varepsilon = 0$ , the driver node selection might be insufficient and it may not be possible to drive the system to a desired target state [85]. Using an error margin buffer increases the driver node selection tolerance and thus selects more driver nodes, which can steer the system to a desired target state. The non-zero values of the driver matrix can be chosen arbitrarily, as long as the constraint in eq. (10) is satisfied. We require that feedback control reaches comparable performance to NODEC in terms of  $r(t)$ , thus we multiply the matrix  $B$  with a positive scalar value  $\zeta$ . Higher absolute values of  $\zeta |B_{i,i}|$  may create control signals that reach the target state in less time at the expense of a higher control energy. As the driver matrix is calculated based on an approximation

of the graph Laplacian pseudoinverse  $L^\dagger$  of a singular system, optimal control guarantees for minimum energy may not always hold. We take the equality of the constraint in eq. (10) to calculate the driver matrix non-zero (control gains) values  $B_{i,i}$ . The target state in eq. (10) is set to  $x_i^* = 0$ .

### 5.1.2 Numerical Simulation Parameters

The control goal is to reach a synchronized state with zero phase difference  $x_i^* - x_j^* = 0$ . To evaluate the system synchronicity, we calculate the order parameter (11), which reaches the maximum value 1 if all oscillators are fully synchronized.

For our numerical experiments, we create an Erdős–Rényi graph  $G(N, p)$  with  $N = 1024$  nodes, mean degree  $\bar{d} \approx 6$ , and link probability  $p = \bar{d}/(N - 1)$ . We generate the driver matrix as in section 5.1.1, and select the non-zero elements as driver nodes. To reduce approximation errors due to the inversion of the Laplacian matrix, we set a buffer margin of  $\varepsilon = 0.1$  when selecting driver nodes. Control signal energy is evaluated with eq. (3). Moreover, we set the coupling constant to  $K = 0.4$  and sample the natural frequencies  $\boldsymbol{\omega}_i$  from a uniform distribution  $\mathcal{U}(-\sqrt{3}, \sqrt{3})$  [86]. This setting results in approximately 70% of the nodes being assigned as driver nodes.

### 5.1.3 NODEC Hyperparameters

We use the system as an input for NODEC by introducing a feedback control neural architecture. Only the current system state  $\mathbf{x}(t)$  is provided as an input for the neural network, similar to the baseline described in section 5.1.1. We use a fully connected architecture as illustrated in fig. 2a. Finally we replace the non-zero elements of  $B$  with 1, as we require the network to learn the control signals per driver node without prior knowledge of the exact control gains, but only the available driver nodes.

Since one of our control goals is to stabilize Kuramoto oscillators in a synchronized state, we need to adapt the training scheme presented in Alg. 1. The loss of synchronization may occur at any point of the trajectory, we train NODEC (see Supplemental Material Alg. 3) in a curriculum learning procedure [15], where NODEC is initially trained on trajectories sampled for low values of  $T$ . The value of  $T$  increases gradually as training proceeds.

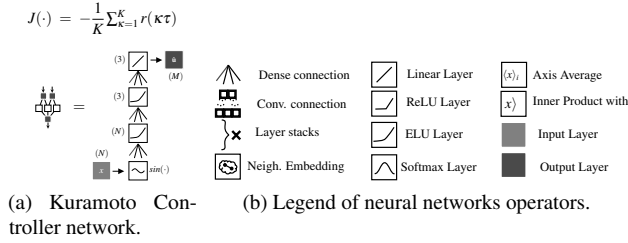


Figure 2: Neural network architecture for controlling Kuramoto oscillators and symbol legend.

The learning process in the beginning of the curriculum, when  $T$  is very low, allows NODEC to learn controls that steer the oscillators through the transient state between synchronicity and no-synchronicity. As  $T$  increases the network also learns controls that preserve the network in the synchronized state.

In feedback control, the target is often to synchronize the system for different initial states [8]. To train the system for more than one initial state, we use a mini-batch-training procedure that samples 8 random initial states per epoch for training. We observed that randomly sampling an initial state from a uniform distribution in  $[0, 2\pi]$  does not improve training performance and fails to learn synchronization. It has been reported in the literature [46] that normally-distributed layer inputs (with zero mean and unit variance) can help neural networks converge faster. Therefore, we decided to sample initial states from a normal distribution with zero mean and unit variance. Our results confirm that learning and convergence improve. Sampling initial states enables us to use mini-batches to speed up and stabilize training as well. In the Kuramoto example we use the Adam optimizer [51] for parameter optimization. The complete training scheme is also illustrated in the Supplemental Material Alg. 3.

#### 5.1.4 Learning Loss Function

For synchronization of Kuramoto oscillators, we consider the order parameter [22]:

$$r(t) = \frac{1}{N} \sqrt{\sum_{i,j} \cos[x_i(t) - x_j(t)]} = \frac{1}{N} \sqrt{\sum_{i,j} e^{i(x_i - x_j)}} \quad (11)$$

to determine the degree of synchronicity. The control loss may also aggregate the order parameter over time, when

the control goals take stability into account. In such a case, one might consider the mean order parameter over time

$$\bar{r}(t) = \frac{1}{T} \int_0^T r(t) dt, \quad (12)$$

which approaches zero if the oscillators are incoherent. By discretizing  $T$  into  $\Xi$  intervals, we can also discretize eq. (12) using

$$\bar{r}(t) = \frac{1}{\Xi} \sum_{\xi=0}^{\Xi} r(\xi\tau), \quad \Xi\tau = T. \quad (13)$$

Equation (13) can be used as a loss function

$$J(\mathbf{x}(0), \dots, \mathbf{x}(T)) = -\bar{r}(t) = -\frac{1}{\Xi} \sum_{\xi=1}^{\Xi} r(\xi\tau) \quad (14)$$

to achieve stable synchronization of coupled oscillators. Such a loss introduces two challenges with respect to the classical MSE loss [14]: (i) it is a macroscopic loss as we do not require to reach a specific state vector  $\mathbf{x}^*$  to minimize eq. (14) and (ii) the loss is calculated over a time interval  $[\tau, T]$ .<sup>2</sup> In our numerical experiments we observed that using such a loss affects numerical stability, especially for long time intervals, e.g. when  $\Xi = 100$  timesteps. Averaging over  $r(\xi t)$  in fig. 3b may smooth out temporal drops of  $r(t)$ , especially for very high values of  $\Xi$ . When such drops occur in sampled training trajectories, NODEC learns to achieve high synchronicity only temporarily. NODEC learns controls that yield highly synchronized stable trajectories similar to FC, when we extend eq. (14) by subtracting the minimum order parameter value  $\min_{t \in [0, T]} r(t)$  over time:

$$J[\{\mathbf{x}(t)\}_0^T] = -\left[ \bar{r}(t) + \min_{t \in [0, T]} r(t) \right]. \quad (15)$$

Introducing the minimum order parameter term increases the stability of the learned control, as the loss creates higher gradients for controls that cause loss of synchronization. NODEC is trained to trajectories that may at maximum reach total time of  $T = 40$ , but is evaluated on trajectories of  $T = 150$ .



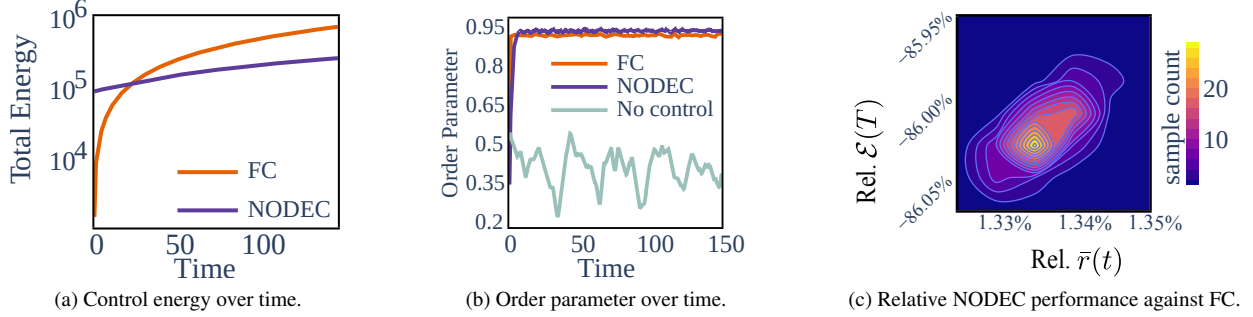


Figure 3: Comparison of NODEC and feedback control in terms of energy and synchronization stability.

### 5.1.5 Results

To test the control performance of NODEC, we first sample an unobserved initial state close to the steady state in accordance with [85]. The initial state values for single sample evaluation (see figs. 3a and 3b) are uniformly sampled within  $+10\%$  of the steady state values, i.e.  $x_i \in [x_i^{\circ}, 0.1x_i^{\circ}]$ , in order to be close to the steady state as proposed in Ref. [85]. We observe that the neural network achieves a target state with larger order parameter values (see fig. 3b) and requires lower energy (see fig. 3a) than the FC baseline. We also observe that NODEC requires higher energy and slightly more time to synchronize the system but less to preserve it, compared to the FC baseline (see fig. 3b and Supplemental Material appdx:fig:osci:loss:zoom).

To determine whether NODEC can achieve synchronization stability regardless of the initial state choice (see fig. 3c) and its proximity to the steady state, we test the trained model on 100 initial states, with values uniformly sampled in  $[0, 2\pi]$ . In fig. 3c the vertical axis represents the relative total energy difference between NODEC and FC for the same initialization  $(\mathcal{E}_{\text{NODEC}}(T) - \mathcal{E}_{\text{FC}}(T)) / \mathcal{E}_{\text{FC}}(T)$ . The horizontal axis represents the mean relative order parameter difference calculated as  $(r_{\text{NODEC}}(T) - r_{\text{FC}}(T)) / r_{\text{FC}}(T)$ . NODEC achieves around 1% higher order parameter values and almost 86% less total control energy for all samples. More sophisticated strategies of adapting the constant term  $\zeta$  in eq. (10) could be applied to adapt the driver matrix values in feedback control. This is, however, out of scope of this

<sup>2</sup>The initial time is omitted ( $\xi = \{1, \dots, Xi\}$  in eq. (14)), since we assume that no control is applied prior to reaching the initial state.

paper. Our results show that NODEC can be adapted to achieve highly synchronized states in Kuramoto dynamics on an Erdős–Rényi graph via feedback control.

## 5.2 Epidemic Spreading and Targeted Interventions

Designing targeted intervention and immunization strategies [19, 79] is important to contain the spread of epidemics. To study the performance of NODEC in such containment tasks, we will use the SIR-X model [61] that extends the SIR model by accounting for quarantine interventions. In our formulation of SIR-X dynamics, we also account for control inputs and network structure. The ‘‘R’’ compartment in our model is used to describe (i) recovered individuals that were infected and acquired immunity and (ii) removed individuals (i.e., susceptible individuals under quarantine who do not interact with anyone else). The corresponding generalized SIR-X dynamics of node  $i$  is described by a set of rate equations:

$$\dot{S}_i(t) = -\beta S_i(t) \sum_j \mathcal{A}_{i,j} I_j(t) - B_i [\kappa_{0,i} + \hat{u}_i(t)] S_i(t) \quad (16a)$$

$$\dot{I}_i(t) = \beta S_i(t) \sum_j \mathcal{A}_{i,j} I_j(t) - \gamma I_i(t) - B_i [\kappa_{0,i} + \hat{u}_i(t)] I_i(t) \quad (16b)$$

$$\dot{R}_i(t) = \gamma I_i(t) + B_i [\kappa_{0,i} + \hat{u}_i(t)] S_i(t) \quad (16c)$$

$$\dot{X}_i(t) = B_i [\kappa_{0,i} + \hat{u}_i(t)] I_i(t) \quad (16d)$$

subject to the conditions that (i) the total population is conserved and (ii) the control budget is bounded above by

$\mathcal{B}$ :

$$\sum_i [S_i + I_i + R_i + X_i] = 1, \quad (17a)$$

$$\sum_i [\kappa_{0,i} + \hat{u}_i(t) \mathbb{1}_{i \in \mathbb{B}}] \leq \mathcal{B}. \quad (17b)$$

Here,  $I_i(t)$ ,  $S_i(t)$ ,  $R_i(t)$ , and  $X_i(t)$  denote the probability of node  $i$  to be infected, susceptible, removed, and contained, respectively. The driver vector element is calculated as  $B_i = \mathbb{1}_{i \in \mathbb{B}}$ . The parameters  $\beta$  and  $\gamma$  are the infection and recovery rates, and  $\kappa_{0,i}$  describes the effect of containment interventions (e.g., mask-usage and distancing). The control signal  $\hat{u}_i(t)$  is applied to driver nodes only and represents dynamic containment measures. We observe that control terms  $B_i [\kappa_{0,i} + \hat{u}_i(t)]$  cancel out when summing over the pairs of eqs. (16a) and (16b) and eqs. (16c) and (16d). These terms are used to model preventive and reactive measures, respectively. For example, susceptible individuals may isolate themselves and completely avoid infection ( $S \rightarrow R$ ) until the pandemic passes (preventive) or infected individuals are quarantined and put to intensive care to avoid spreading and recover ( $I \rightarrow X$ ) (reactive measure). The indicator function  $\mathbb{1}_{i \in \mathbb{B}}$  is 1 if node  $i$  is a driver node (i.e., individuals that are willing to participate in the containment measures) and 0 otherwise. Driver nodes are selected with the maximum matching method proposed in section 3.1. In our simulations, we assume that the epidemic originates from a localized part in the graph and we minimize the proposed epidemic loss in eq. (19).

### 5.2.1 Control Baselines

A baseline that takes structural node properties (e.g., node degree or centrality) into the account, may be a good baseline for structural-heterogeneous graphs, but not for regular structures like lattices. Clearly, a weak baseline (RND) would be assigning random control inputs to driver nodes with  $k_{0,j} = 0, u_j(t) = \mathcal{B}c_j / \sum_{j=0}^M c_j, c_j \sim \mathcal{U}(0, 1)$ . However, a targeted constant control baseline (TCC), which in the presence of an ‘‘oracle’’ assigns constant control inputs  $k_0 = \mathcal{B}/M$  to every driver node in  $G^*$ , is a strong baseline for constant control. The budget constraint [see eq. (17b)], the high number of nodes connecting  $G^*$  to the rest of lattice graph and constraint to only control driver nodes does not allow to create dense ‘‘impenetrable walls’’ of containment, as an infection can still pass through contained

nodes at a lower rate. As TCC is a static control, it already protects the driver nodes from  $t = 0$  on, so TCC-controlled nodes will be infected very slowly. Assigning all budget to all driver nodes of interest also minimizes wasted ‘‘containment’’ budget. Still, distributing more budget to a smaller number of nodes increases the L2 norm of the control, making controls very expensive when considering quadratic energy costs. To have a control with less energy, it is important to distribute the budget to more nodes, therefore enabling more global containment and less constant containment on the target sub-graph.

We also study the performance of dynamic control baselines  $k_{0,i} = 0$ , such as continuous-action RL, with fully-connected neural networks or our variant (see Figure 4) as policy architectures, which we discuss further in the following section. Only one of the three evaluated training routines of RL provided high-performance results. We tested: SAC [40], TD3 [36], and A2C [67], but we report only the results of TD3 which were more competitive with respect to NODEC. To allow RL to tackle the SIR-X control problem, we first implement SIR-X dynamics as an RL environment. The input of the RL is the tensor of all SIR-X states at time  $t$ . We consider an observation space, which includes continuous values in  $[0, 1]$  and has dimension  $4 \times N$ . RL actions are continuous values for each driver node, so the policies are continuous policies over  $M$  nodes in  $\mathbb{R}^M$ . Once the controls are passed to the environment, a pre-processing operation takes place to convert the RL action into valid control signals. This operation is explained in detail within the section 5.2.3 and is illustrated in the decision network of fig. 4. Reinforcement learning is allowed to provide new control signals to (interact with) the environment in a fixed discrete time interaction interval  $\Delta t = 10^{-2}$  during training. Lower interaction intervals were also considered, but required longer training and did not seem to improve performance. For reinforcement learning, we need to express the control goal as a reward function which is used for the approximation of action value function within the RL framework. We tested several reward designs and we describe this process in the Supplemental Material appendix B.1, but we observed best performance with the following reward function:

$$\rho(t) = \begin{cases} 0, & \text{if } \bar{I}_{G^*}(t) \leq \max_{\tau < t} (\bar{I}_{G^*}(\tau)) \\ -\bar{I}_{G^*}^2(t) + (\max_{\tau < t} \bar{I}_{G^*}(\tau))^2, & \text{otherwise} \end{cases} \quad (18)$$

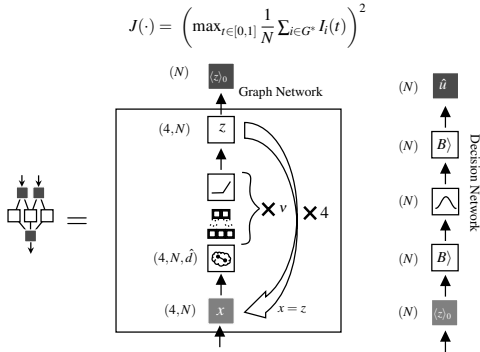


Figure 4: NODEC architecture for controlling SIRX dynamics.

### 5.2.2 Numerical Simulation

To determine the target time  $T$ , we observe the SIR-X dynamics ( $\beta = 6$  and  $\gamma = 1.8$ ) on a  $32 \times 32$  lattice without control and set its value to the time at which the mean infection over all nodes is approximately zero. Initially, the epidemic starts from a deterministic selection of nodes in the upper-right quadrant. For all control strategies, the budget (maximal number of control interventions) is  $B = 600$ . Given that Reinforcement Learning takes considerably longer to converge and that we were required to perform a much more extensive hyper parameter search, we showcase our experiments only on the lattice graph and a single initial state. Our control goal is to contain epidemic outbreaks (i.e., “flattening” the infection curve) in the subgraph  $G^*$ , which is located in the bottom-left quadrant (see Figure 6). All baselines are compared under interaction interval of  $\Delta t = 10^{-3}$ .

### 5.2.3 NODEC Hyperparameters

From a technical perspective, the SIR-X dynamics introduce extra state variables. Therefore, fully-connected layers will require one to estimate considerably more parameters. We observe that neither NODEC nor RL converged to a high-performance solution when using fully-connected layers, and we thus omit these results. Furthermore, the control task requires the network to optimize a loss that is not calculated over whole graph, but rather on a specific sub-graph. NODEC has no direct information on which nodes are part of subgraph  $G^*$ . The informa-

tion is provided via the minimization of the learning loss-function in eq. (19). Back-propagation happens at time  $t^* = \arg \max_{t \leq T} J(I_{G^*}(t))$ . This time is approximated by preserving a sample of states when using the ODEsolve, and picking the maximum observed peak infection from that sample. As the existing neural architectures discussed in section 5.1.3 did not perform well, we switch to an architecture that includes the graph structures. We use a graph neural network (GNN) that contains all learnable parameters (see fig. 4). The same GNN architecture is implemented in the RL baselines as the policy network. GNN encountered fewer numerical instabilities during training and allowed for efficient learning without curriculum procedures. We use a training procedure for SIR-X control as shown in Supplemental Material Alg. 4 that preserves the best performing model in terms of loss.

The input state has 4 state variables that are used as convolution channels. For each channel, we create a neighborhood embedding matrix  $\Psi$ , a  $N \times \hat{d}$  matrix, where  $\hat{d}$  is the maximum network degree. Each value of the neighborhood embedding contains the state variable of a neighbor  $j: \mathcal{A}_{i,j} \neq 0$ . If the node  $i$  has less than  $\hat{d}$  neighbors, the remaining elements of the  $i$ -th row of  $\Psi$  have value 0. The collection of neighborhood embedding matrices are provided to a stack of  $v$  convolutional layers of  $3 \times 1$  kernel size and 5 output channels, which consecutively reduce the input width from  $\hat{d}$  to 1, while preserving the height  $N$ . As indicated, the number of stacked convolutional layers depends on the maximum degree of the network. For a non-periodical square lattice with maximum degree  $\hat{d} = 4$  we use  $v = 1$  convolutional layers. Once the last layer is reached, the channels are reduced to 4 and a hidden output  $z$  is produced. Then the feed-forward process is repeated 4 times by setting the input  $x = z$  to simulate the message propagation technique often used in GNNs [80]. After the last message propagation is finished, the mean over the channels is calculated, yielding a vector of scalar values over all nodes  $\langle z \rangle_0$ .

The decision network contains operations that enforce the budget and driver constraints. It is included inside the NODEC architecture and RL environment. Transfer learning [71] between NODEC and RL can be achieved by pre-training the GNN network with NODEC and then using it as an RL policy. RL achieves the same performance as NODEC when transfer learning was tested. Further fine tuning of the pre-trained policy with RL does not im-

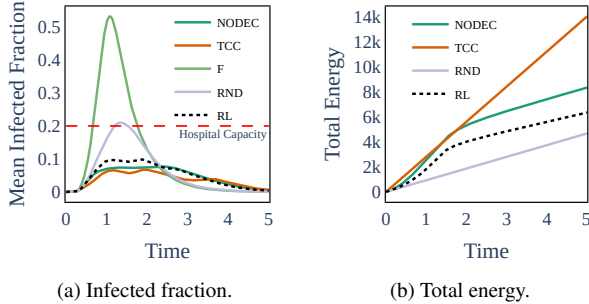


Figure 5: SIR-X control evaluation. Nodec versus base-lines: reinforcement learning (RL), targeted constant control (TCC), random constant control (RND), and free dynamics with no control (F).

prove performance of NODEC in this setting, but transfer learning indicates a possible future extension of combining model-based training with real-world model-free fine tuning.

#### 5.2.4 Learning Loss

To account for control signals in such dynamics, we introduce an extra state variable  $X_i(t)$ , which denotes the part of a population on node  $i$  at time  $t$  that is subject to containment policies that delay or prevent infection [61]. The control goal is to “flatten” the curve, i.e. to delay and minimize the mean infected-fraction over nodes in the subgraph  $G^*$ , which has no overlap with the part of the graph containing the initial spreading seed. Based on these control goals, we formulate the following loss function:

$$J(I(t)) = [\max_{t \leq T} \bar{I}_{G^*}(t)]^2, \quad (19)$$

where  $\bar{I}_{G^*}$  denotes the mean fraction of infected individuals in  $G^*$ . This goal is clearly macroscopic, as we do not know the exact feasible state that minimizes such loss. Similar to eq. (15), it requires loss calculations over a time interval. Moreover, this loss is not calculated over the whole state vector  $\mathbf{x}$  but only on a single state variable  $i$  and target subgraph  $G^*$ . Intuitively, one would trivially achieve the proposed goal if there are no further constraints. If nodes that connect the subgraph  $G^*$  to the rest of the graph cannot be controlled efficiently, then achieving the

control goal becomes non-trivial. Tackling the outlined epidemic control problem allows us to evaluate NODEC on a complex control task (see section 5.2.5) with applications in disease control.

#### 5.2.5 Results

Our main results are summarized in fig. 5 and Table 1 and indicate similar superior performance of TCC and NODEC compared to the other control strategies, but with lower energy costs for NODEC. In Figure 5, we observe that NODEC is providing strong protection with total energy costs that are not as high as TCC (see Table 1). If we assume that the proposed system will reach maximum hospital capacity at 20% of the infected fraction in the target subgraph, we observe that TCC, RL, and NODEC are sustainable control strategies. In fig. 5a and Table 1, NODEC underperforms TCC with approximately 1% higher maximum infection fraction, but requires almost 41% less control energy. The effectiveness of the control can be attributed to the adaptive nature of NODEC. The other adaptive baseline, RL requires around 54% less energy than TCC but allows for 2.1% higher peak infection compared to NODEC. The effectiveness of targeted adaptive controls in time can be used to model and examine the effectiveness of proposed real-world long-term pandemic control strategies, such as rolling lockdowns [1] and/or vaccine allocation [75].

NODEC achieves better performance at the cost of higher energy compared to RL. Reinforcement learning is often described as “model-free” and addresses the (i) prediction problem and (ii) control problem [90]. We note that RL approaches may suffer from credit assignment challenges, where a reward signal is uninformative regarding the specific actions (especially in terms of time) that help reach the goal [89]. However, even after testing different reward designs and parameters settings, no RL framework managed to perform better than our baselines. It may be possible that extensive reward engineering, and other model upgrades may lead to a better performance. In contrast to RL, the proposed NODEC is not model-free and the underlying gradient descent is directly calculated from the loss function. Therefore, we do not need to consider value prediction and credit assignment. It is possible to design a model-free NODEC by learning the underlying system dynamics simultaneously with control similar to

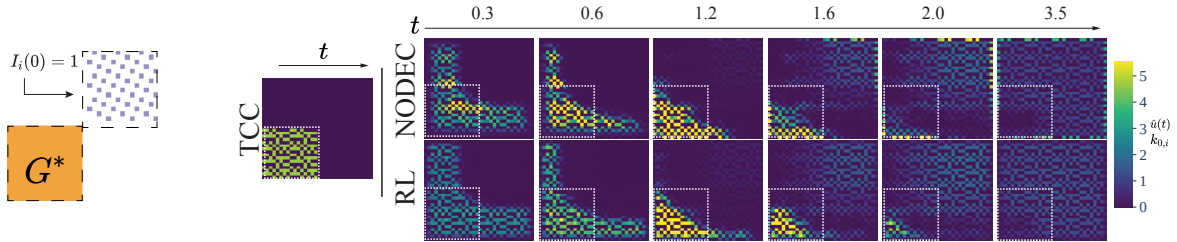


Figure 6: Initial infection, target subgraph, and control trajectories for SIR-X dynamics. Colorscale plots represent 99.5% of the presented values for dynamics with NODEC controls.

Ref. [44], which could be an interesting future extension of our work.

Table 1: Total energy  $\mathcal{E}(T)$  and peak infection  $\max_t(\bar{I}(t))$  achieved by different epidemic spreading control methods.

Control	Peak Infection	Total Energy
TCC	0.068	14062.6
NODEC	0.078	8356.6
RL	0.099	6358.0
RND	0.210	4688.9
F	0.532	0.0

The spread of the epidemic, target subgraph, and controls of the main baselines are illustrated in fig. 6. For RL and NODEC, we observe that after some time controls reemerge in areas that were initially infected. This is an architecture artifact as the network calculates controls by multiplying the budget with a softmax output to always distribute all available budget to the network. This artifact also exists in other baselines, as all baselines distribute the available budget on the selected participants across time.

## 6 Discussion and Conclusion

Neural ODE control approximates dynamical systems based on observations of the system-state evolution and determines control inputs according to pre-defined target states. Contrary to Ref. [27] that parameterizes the derivative of hidden states using neural networks, our neural-ODE systems describe controlled dynamical systems on graphs. In general, neural networks are able to approximate any control input as long as they satisfy correspond-

ing universal approximation theorems. However, in practice, NODEC needs to deal with different numerical hurdles such as large losses and stiffness problems of the underlying ODE systems. By testing NODEC on various graph structures and dynamical systems, we provide evidence that these hurdles can be overcome with appropriate choices of both hyperparameters and numerical ODE solvers.

Future studies may study the effectiveness of NODEC under additional constraints such as partial observability and delayed and noisy controls.

## Acknowledgements

L.B. acknowledges financial support from the SNF (P2EZP2\_191888). N.A.-F. has been funded by the European Program scheme 'INFRAIA-01- 2018-2019: Research and Innovation action', grant agreement #871042 'SoBigData++: European Integrated Infrastructure for Social Mining and Big Data Analytics'. T.A. received financial support from the LCM – K2 Center within the framework of the Austrian COMET-K2 program.

## Data Availability Statement

Figures and tables are available within the article and also the Supplemental Material Document. The experiment data that support the findings of this study are openly available in the NODEC IEEE Dataport repository[5] at <https://dx.doi.org/10.21227/gdqj-am79>. The code that fully reproduces the above experiments is found as a code ocean capsule [7] at <https://codeocean>.

com/capsule/1934600/tree. A fully functioning code library [6] written in python for neural network control with NODEC is found at <https://github.com/asikist/nnc> with coding examples and more applications.

## References

- [1] D. Acemoglu, V. Chernozhukov, I. Werning, and M. D. Whinston. Optimal targeted lockdowns in a multi-group sir model. *NBER Working Paper*, 27102, 2020.
- [2] B. Amos, I. Jimenez, J. Sacks, B. Boots, and J. Z. Kolter. Differentiable mpc for end-to-end planning and control. In *Advances in Neural Information Processing Systems*, pages 8289–8300. Curran Associates, Inc., 2018.
- [3] H. Andersson and T. Britton. *Stochastic epidemic models and their statistical analysis*, volume 151. Springer Science & Business Media, 2012.
- [4] N. Antulov-Fantulin, A. Lančić, T. Šmuc, H. Štefančić, and M. Šikić. Identification of patient zero in static and temporal networks: Robustness and limitations. *Physical Review Letters*, 114(24):248701, 2015.
- [5] T. Asikis, L. Böttcher, and N. Antulov-Fantulin. Data repository for all nodec experiments, 2020.
- [6] T. Asikis, L. Böttcher, and N. Antulov-Fantulin. Github repository for neural network control, 2020.
- [7] T. Asikis, L. Böttcher, and N. Antulov-Fantulin. Code ocean capsule for reproducing all nodec experiments, 2021.
- [8] K. J. Åström and R. M. Murray. *Feedback systems: an introduction for scientists and engineers*. Princeton Univeristy Press, 2010.
- [9] A.-L. Barabási and R. Albert. Emergence of scaling in random networks. *Science*, 286(5439):509–512, 1999.
- [10] A. Barrat, M. Barthelemy, and A. Vespignani. *Dynamical processes on complex networks*. Cambridge university press, 2008.
- [11] B. Barzel and A.-L. Barabási. Universality in network dynamics. *Nature Physics*, 9(10):673–681, 2013.
- [12] A. G. Baydin, B. A. Pearlmutter, A. A. Radul, and J. M. Siskind. Automatic differentiation in machine learning: a survey. *Journal of Machine Learning Research*, 18(1):5595–5637, 2017.
- [13] R. E. Bellman and S. E. Dreyfus. *Applied dynamic programming*. Princeton university press, 2015.
- [14] A. Bemporad, M. Morari, V. Dua, and E. N. Pistikopoulos. The explicit linear quadratic regulator for constrained systems. *Automatica*, 38(1):3–20, 2002.
- [15] Y. Bengio, J. Louradour, R. Collobert, and J. Weston. Curriculum learning. In *International Conference on Machine Learning*, pages 41–48, 2009.
- [16] S. Bhasin, R. Kamalapurkar, M. Johnson, K. G. Vamvoudakis, F. L. Lewis, and W. E. Dixon. A novel actor–critic–identifier architecture for approximate optimal control of uncertain nonlinear systems. *Automatica*, 49(1):82–92, 2013.
- [17] U. Biccari and E. Zuazua. A stochastic approach to the synchronization of coupled oscillators. *Frontiers in Energy Research*, 8:115, 2020.
- [18] C. Bick, M. J. Panaggio, and E. A. Martens. Chaos in kuramoto oscillator networks. *Chaos: An Interdisciplinary Journal of Nonlinear Science*, 28(7):071102, 2018.
- [19] L. Böttcher, J. Andrade, and H. J. Herrmann. Targeted recovery as an effective strategy against epidemic spreading. *Scientific Reports*, 7(1):1–7, 2017.
- [20] L. Böttcher, N. Antulov-Fantulin, and T. Asikis. Implicit energy regularization of neural ordinary-differential-equation control. *arXiv preprint arXiv:2103.06525*, 2021.

- [21] L. Böttcher, H. J. Herrmann, and H. Gersbach. Clout, activists and budget The road to presidency. *PLOS ONE*, 13(3), 2018.
- [22] M. Brede. Locals vs. global synchronization in networks of non-identical kuramoto oscillators. *The European Physical Journal B*, 62(1):87–94, 2008.
- [23] D. Brockmann and D. Helbing. The hidden geometry of complex, network-driven contagion phenomena. *Science*, 342(6164):1337–1342, 2013.
- [24] M. A. Bucci, O. Semeraro, A. Allauzen, G. Wisniewski, L. Cordier, and L. Mathelin. Control of chaotic systems by deep reinforcement learning. *Proceedings of the Royal Society A*, 475(2231), 2019.
- [25] A. Camacho, O. Chen, S. Sanner, and S. A. McIlraith. Non-markovian rewards expressed in ltl: guiding search via reward shaping. In *Annual Symposium on Combinatorial Search*, 2017.
- [26] C. Castellano and R. Pastor-Satorras. Thresholds for epidemic spreading in networks. *Physical Review Letters*, 105(21):218701, 2010.
- [27] R. T. Q. Chen, Y. Rubanova, J. Bettencourt, and D. Duvenaud. Neural ordinary differential equations. *Advances in Neural Information Processing Systems*, 2018.
- [28] C. Commault, J.-M. Dion, and J. W. van der Woude. Characterization of generic properties of linear structured systems for efficient computations. *Kybernetika*, 38(5):503–520, 2002.
- [29] S. P. Cornelius, W. L. Kath, and A. E. Motter. Realistic control of network dynamics. *Nature Communications*, 4(1):1–9, 2013.
- [30] D. Cumin and C. Unsworth. Generalising the kuramoto model for the study of neuronal synchronisation in the brain. *Physica D: Nonlinear Phenomena*, 226(2):181–196, 2007.
- [31] D. Delpini, S. Battiston, M. Riccaboni, G. Gabbi, F. Pammolli, and G. Caldarelli. Evolution of controllability in interbank networks. *Scientific Reports*, 3(1), Apr. 2013.
- [32] F. Dorfler and F. Bullo. Synchronization and transient stability in power networks and nonuniform kuramoto oscillators. *SIAM Journal on Control and Optimization*, 50(3):1616–1642, 2012.
- [33] S. N. Dorogovtsev, A. V. Goltsev, and J. F. Mendes. Critical phenomena in complex networks. *Reviews of Modern Physics*, 80(4):1275, 2008.
- [34] W. H. Fleming and H. M. Soner. *Controlled Markov processes and viscosity solutions*, volume 25. Springer Science & Business Media, 2006.
- [35] H. Frankowska. Nonsmooth solutions of hamilton-jacobi-bellman equation. In *Modeling and Control of Systems*, pages 131–147. Springer-Verlag, 1989.
- [36] S. Fujimoto, H. Hoof, and D. Meger. Addressing function approximation error in actor-critic methods. In *International Conference on Machine Learning*, pages 1587–1596, 2018.
- [37] M. R. Garey and D. S. Johnson. *Computers and intractability*, volume 174. Freeman San Francisco, 1979.
- [38] M. Girvan and M. E. Newman. Community structure in social and biological networks. *Proceedings of the National Academy of Sciences*, 99(12):7821–7826, 2002.
- [39] J. P. Gleeson. Binary-state dynamics on complex networks: Pair approximation and beyond. *Physical Review X*, 3(2):021004, 2013.
- [40] T. Haarnoja, A. Zhou, P. Abbeel, and S. Levine. Soft actor-critic: Off-policy maximum entropy deep reinforcement learning with a stochastic actor. In *International Conference on Machine Learning*, pages 1861–1870, 2018.
- [41] B. Hanin and M. Sellke. Approximating continuous functions by relu nets of minimal width. *arXiv preprint arXiv:1710.11278*, 2017.
- [42] M. L. Hautus. Controllability and observability conditions of linear autonomous systems. In *Indagationes Mathematicae (Proceedings)*, volume 72, pages 443–448, 1969.

- [43] M. Hoferer, L. Böttcher, H. J. Herrmann, and H. Gersbach. The impact of technologies in political campaigns. *Physica A: Statistical Mechanics and its Applications*, 538:122795, 2020.
- [44] P. Holl, V. Koltun, and N. Thuerey. Learning to control pdes with differentiable physics. In *International Conference on Learning Representations*, 2020.
- [45] C. Hua and X. Guan. Adaptive control for chaotic systems. *Chaos, Solitons & Fractals*, 22(1):55–60, 2004.
- [46] S. Ioffe and C. Szegedy. Batch normalization: Accelerating deep network training by reducing internal covariate shift. In *International Conference on Machine Learning*, pages 448–456, 2015.
- [47] R. E. Kalman et al. Contributions to the theory of optimal control. *Boletín de la Sociedad Matemática Mexicana*, 5(2):102–119, 1960.
- [48] M. I. Kamien and N. L. Schwartz. Sufficient conditions in optimal control theory. *Journal of Economic Theory*, 3(2):207–214, 1971.
- [49] P. Kidger, R. T. Q. Chen, and T. Lyons. "hey, that's not an ode": Faster ode adjoints with 12 lines of code. *arXiv preprint arXiv:2009.09457*, 2020.
- [50] P. Kidger, J. Morrill, J. Foster, and T. Lyons. Neural controlled differential equations for irregular time series. In *Advances in Neural Information Processing Systems*. Curran Associates, Inc., 2020.
- [51] D. P. Kingma and J. Ba. Adam: A method for stochastic optimization. In Y. Bengio and Y. LeCun, editors, *International Conference on Learning Representations, ICLR 2015, San Diego, CA, USA, May 7-9, 2015, Conference Track Proceedings*, 2015.
- [52] B. Kiumarsi, K. G. Vamvoudakis, H. Modares, and F. L. Lewis. Optimal and autonomous control using reinforcement learning: A survey. *IEEE Transactions on Neural Networks and Learning Systems*, 29(6):2042–2062, 2017.
- [53] Y. Kuramoto. Self-entrainment of a population of coupled non-linear oscillators. In *International Symposium on Mathematical Problems in Theoretical Physics*, pages 420–422. Springer, 1975.
- [54] J. Leskovec, D. Chakrabarti, J. Kleinberg, C. Faloutsos, and Z. Ghahramani. Kronecker graphs: An approach to modeling networks. *Journal of Machine Learning Research*, 11(Feb):985–1042, 2010.
- [55] F. Lewis, S. Jagannathan, and A. Yesildirak. *Neural network control of robot manipulators and nonlinear systems*. CRC press, 2020.
- [56] C.-T. Lin. Structural controllability. *IEEE Transactions on Automatic Control*, 19(3):201–208, 1974.
- [57] B. G. Liptak. *Instrument Engineers' Handbook, Volume Two: Process Control and Optimization*. CRC press, 2018.
- [58] Y.-Y. Liu and A.-L. Barabási. Control principles of complex systems. *Reviews of Modern Physics*, 88(3):035006, 2016.
- [59] Y.-Y. Liu, J.-J. Slotine, and A.-L. Barabási. Controllability of complex networks. *Nature*, 473(7346):167–173, 2011.
- [60] J. Lygeros. On reachability and minimum cost optimal control. *Automatica*, 40(6):917–927, 2004.
- [61] B. F. Maier and D. Brockmann. Effective containment explains subexponential growth in recent confirmed covid-19 cases in china. *Science*, 368(6492):742–746, 2020.
- [62] Y. L. Maistrenko, O. V. Popovych, and P. A. Tass. Chaotic attractor in the kuramoto model. *International Journal of Bifurcation and Chaos*, 15(11):3457–3466, 2005.
- [63] O. L. Mangasarian. Sufficient conditions for the optimal control of nonlinear systems. *SIAM Journal on Control*, 4(1):139–152, 1966.
- [64] O. Mayr. The origins of feedback control. *Scientific American*, 223(4):110–119, 1970.



- [65] E. McShane. The calculus of variations from the beginning through optimal control theory. *SIAM Journal on Control and Optimization*, 27(5):916–939, 1989.
- [66] E. Mizutani and S. E. Dreyfus. Two stochastic dynamic programming problems by model-free actor-critic recurrent-network learning in non-markovian settings. In *IEEE International Joint Conference on Neural Networks (IEEE Cat. No. 04CH37541)*, volume 2, pages 1079–1084. IEEE, 2004.
- [67] V. Mnih, A. P. Badia, M. Mirza, A. Graves, T. Lillicrap, T. Harley, D. Silver, and K. Kavukcuoglu. Asynchronous methods for deep reinforcement learning. In *International Conference on Machine Learning*, pages 1928–1937, 2016.
- [68] J. E. Moyal. Stochastic processes and statistical physics. *Journal of the Royal Statistical Society. Series B (Methodological)*, 11(2):150–210, 1949.
- [69] M. Newman. *Networks*. Oxford university press, 2018.
- [70] A. Olshevsky. Minimal controllability problems. *IEEE Transactions on Control of Network Systems*, 1(3):249–258, 2014.
- [71] S. J. Pan and Q. Yang. A survey on transfer learning. *IEEE Transactions on knowledge and data engineering*, 22(10):1345–1359, 2009.
- [72] B. Pang, Z.-P. Jiang, and I. Mareels. Reinforcement learning for adaptive optimal control of continuous-time linear periodic systems. *Automatica*, 118:109035, 2020.
- [73] R. Pastor-Satorras, C. Castellano, P. Van Mieghem, and A. Vespignani. Epidemic processes in complex networks. *Reviews of Modern Physics*, 87:925–979, Aug 2015.
- [74] A. Paszke, S. Gross, F. Massa, A. Lerer, J. Bradbury, G. Chanan, T. Killeen, Z. Lin, N. Gimeshein, L. Antiga, et al. Pytorch: An imperative style, high-performance deep learning library. In *Advances in Neural Information Processing Systems*, pages 8026–8037. Curran Associates, Inc., 2019.
- [75] V. M. Preciado, M. Zargham, C. Enyioha, A. Jadbabaie, and G. Pappas. Optimal vaccine allocation to control epidemic outbreaks in arbitrary networks. In *IEEE Conference on Decision and Control*, pages 7486–7491. IEEE, 2013.
- [76] D. J. D. S. Price. Networks of scientific papers. *Science*, pages 510–515, 1965.
- [77] F. A. Rodrigues, T. K. D. Peron, P. Ji, and J. Kurths. The kuramoto model in complex networks. *Physics Reports*, 610:1–98, 2016.
- [78] J. Ruths and D. Ruths. Control profiles of complex networks. *Science*, 343(6177):1373–1376, 2014.
- [79] M. Salathé and J. H. Jones. Dynamics and control of diseases in networks with community structure. *PLOS Computational Biology*, 6(4), 2010.
- [80] F. Scarselli, M. Gori, A. C. Tsoi, M. Hagenbuchner, and G. Monfardini. The graph neural network model. *IEEE Transactions on Neural Networks*, 20(1):61–80, 2008.
- [81] A. M. Schäfer and H. G. Zimmermann. Recurrent neural networks are universal approximators. In *International Conference on Artificial Neural Networks*, pages 632–640. Springer, 2006.
- [82] D. Schoenwald and U. Ozguner. Optimal control of feedback linearizable systems. In *[1992] Proceedings of the 31st IEEE Conference on Decision and Control*, pages 2033–2034. IEEE, 1992.
- [83] J. Sethna et al. *Statistical mechanics: entropy, order parameters, and complexity*, volume 14. Oxford University Press, 2006.
- [84] L. F. Shampine. *Numerical solution of ordinary differential equations*. Routledge, 2018.
- [85] P. S. Skardal and A. Arenas. Control of coupled oscillator networks with application to microgrid technologies. *Science Advances*, 1(7), 2015.
- [86] P. S. Skardal and A. Arenas. On controlling networks of limit-cycle oscillators. *Chaos: An Interdisciplinary Journal of Nonlinear Science*, 26(9), 2016.

- [87] E. D. Sontag and H. Siegelmann. On the computational power of neural nets. *Journal of Computer and System Sciences*, 50:132–150, 1995.
- [88] M. H. Stone. The generalized weierstrass approximation theorem. *Mathematics Magazine*, 21(5):237–254, 1948.
- [89] R. S. Sutton. Temporal credit assignment in reinforcement learning. *PhD dissertation*, 1985.
- [90] R. S. Sutton and A. G. Barto. *Reinforcement learning: An introduction*. MIT press, 2018.
- [91] S. Thiébaux, C. Gretton, J. Slaney, D. Price, and F. Kabanza. Decision-theoretic planning with non-markovian rewards. *Journal of Artificial Intelligence Research*, 25:17–74, 2006.
- [92] N. G. Van Kampen. *Stochastic processes in physics and chemistry*, volume 1. Elsevier, 1992.
- [93] D. J. Watts and S. H. Strogatz. Collective dynamics of ‘small-world’ networks. *Nature*, 393(6684):440, 1998.
- [94] A. W. Wijayanto and T. Murata. Flow-aware vertex protection strategy on large social networks. In *2017 IEEE/ACM International Conference on Advances in Social Networks Analysis and Mining (ASONAM)*, pages 58–63. IEEE, 2017.
- [95] T. Yamada and L. R. Foulds. A graph-theoretic approach to investigate structural and qualitative properties of systems: A survey. *Networks*, 20(4):427–452, 1990.
- [96] G. Yan, J. Ren, Y.-C. Lai, C.-H. Lai, and B. Li. Controlling complex networks: How much energy is needed? *Physical Review Letters*, 108(21):218703, 2012.
- [97] M. S. Yeung and S. H. Strogatz. Time delay in the kuramoto model of coupled oscillators. *Physical Review Letters*, 82(3):648, 1999.
- [98] S. J. Yoo, J. B. Park, and Y. H. Choi. Stable predictive control of chaotic systems using self-recurrent wavelet neural network. *International Journal of Control, Automation and Systems*, 3(1):43–55, 2005.
- [99] D.-X. Zhou. Universality of deep convolutional neural networks. *Applied and Computational Harmonic Analysis*, 48(2):787–794, 2020.
- [100] X. Zhou. Maximum principle, dynamic programming, and their connection in deterministic control. *Journal of Optimization Theory and Applications*, 65(2):363–373, 1990.

# Supplemental Material

## A Kuramoto Oscillators

### A.1 Curriculum Learning

A curriculum learning procedure is used to train Kuramoto models. The algorithm is illustrated below in Alg. 3.

---

**Algorithm 3:** Curriculum training process of NODEC. A procedure that gradually increases total time is introduced in this algorithm. Here we present a stochastic procedure, but a deterministic procedure is also possible.

---

```

Result:  $\mathbf{w}$ 
1 Init:  $\mathbf{x}_0, \mathbf{w}, f(\cdot), \text{ODESolve}(\cdot), \text{Optimizer}(\cdot), J(\cdot), \mathbf{x}^*$ ;
2 Params:  $\eta, \text{epochs}, \text{stepSize}$ ;
3  $\text{epoch} \leftarrow 0$ ;
4  $T \leftarrow 0$  while  $\text{epoch} < \text{epochs}$  do
5    $t \leftarrow 0$ ;
6    $c \leftarrow \mathcal{U}(0, 1)$ ;
7    $T \leftarrow T + 2 \cdot c$ ;
8    $\mathbf{x} \sim \mathcal{N}_N(0_1^N, 1_1^N)$ ;
9    $\text{meanLoss} \leftarrow \text{List}$   $\text{minLoss} \leftarrow \infty$ 
10  while  $t < T$  do
11     $\mathbf{x}_t, \text{hasNumInstability} \leftarrow$ 
       $\text{ODESolve}(\mathbf{x}, t, t + \text{stepSize}, f, \hat{\mathbf{u}}(\mathbf{x}; \mathbf{w}))$ ;
12    if Not  $\text{hasNumInstability}$  then
13       $\text{meanLoss} \leftarrow (\text{stepSize}/T) \cdot J(\mathbf{x}_t, \mathbf{x}^*)$ ;
14      if  $\text{minLoss} > J(\mathbf{x}_t, \mathbf{x}^*)$  then
15         $\text{minLoss} \leftarrow J(\mathbf{x}_t, \mathbf{x}^*)$ ;
16      end
17    end
18     $t \leftarrow t + \text{stepSize}$ ;
19  end
20   $\text{Optimizer.update}(\mathbf{w}, -(\text{meanLoss} + \text{minLoss}))$ ;
21 end

```

---

### A.2 Synchronization Loss Before Convergence

In this section, we describe one of the results presented in fig. 3b in more detail. We observe that NODEC takes more time to converge to a synchronized state in the example illustrated in fig. 7. We also observe that NODEC requires a higher amount

of control energy before reaching the synchronized state fig. 3a. Once synchronicity is reached, the neural network can adapt and produce lower energy controls. This might not be the case for feedback control, which has a constant term  $\zeta$  multiplied by the driver matrix values.

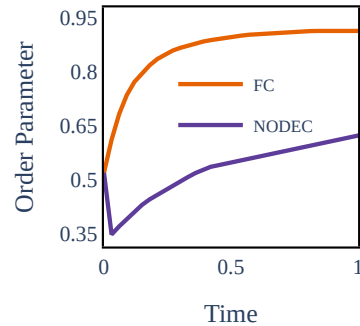


Figure 7: Early order parameter values based on fig. 3b.

## B SIRX

### B.1 Reinforcement Learning

In this section, we focus on the technical details of the RL baseline we used in the main paper. Reinforcement learning is often described as “model-free” and addresses the (i) prediction problem and (ii) control problem [90]. We note that RL approaches may suffer from credit assignment challenges, where a reward signal is uninformative regarding the specific actions (especially in terms of time) that help reach the goal [89]. In contrast to RL, the proposed NODEC is not model-free and the underlying gradient descent is directly calculated from the loss function. Therefore, we do not need to consider value prediction and credit assignment. It is possible to design a model-free NODEC by learning the underlying system dynamics simultaneously with control, which could be an interesting future extension of our work. Note that a direct performance comparison between RL and NODEC in terms of target loss may be considered unfair especially towards RL methods, unless extensive hyper-parameter optimization is performed beforehand.

We first implement SIRX dynamics as an RL environment. The softmax operation and budget assignment discussed in Section 5.2.3 take place in the environment and RL computes the softmax logit values over all driver nodes. Reinforcement learning is allowed to interact with the environment in a fixed interaction interval  $\Delta t = 10^{-2}$ , similar to NODEC. A2C and SAC

implementations are taken from StableBaselines3<sup>3</sup>. Both implementations were tested for different parameter sets and trained for at least 50000 steps. Unfortunately, no implementation was able to “flatten the curve” considerably better than random control. Next, we use the TD3 implementation from Tianshu<sup>4</sup>, which currently showcases high-speed benchmarks and allows more customization of policy/critic architectures. The corresponding RL training takes around 17 seconds per epoch, whereas NODEC takes approximately 5.5 seconds per epoch. Neither TD3 or NODEC fully utilized the GPU in terms of computing and memory resources, often staying below 50% of usage, while memory utilization usually was below 10GB per method.

We show an overview of the hyperparameters that we use to train TD3 in Table 2. For more detailed explanations of these hyperparameters, see Ref. [36] and the Tianshu documentation<sup>5</sup>. Several baseline architectures in RL frameworks are often fully-connected multilayer perceptrons. Still, we observe that the graph neural network presented in fig. 4 was more efficient in converging rewards in less computation time. We trained all models for 100 epochs and stored and evaluated the best model. In SAC and A2C, one training environment was used, whereas TD3 was sampling from two independent environments simultaneously due to its computational speed.

In terms of parameters both the TD3 policy network and NODEC GNN have exactly the same learning parameters (weights), but training is very different, as the gradient flows presented in Figure 1 and Algs. 1 and 2 cannot happen. The value function is now used for the calculation of similar gradients by predicting the cumulative reward signal. We studied several possible reward designs, and in the end we rigorously tested the following rewards:

The first reward signal we tested is calculated based on the mean number of infected nodes belonging to the target sub-graph  $\bar{I}_{G^*}(t)$  at time  $t$ :

$$\rho_1(t) = -(\bar{I}_{G^*}(t))^2 \Delta t. \quad (20)$$

Although this reward seemingly provides direct feedback for an action, it also leads to several challenges. First, it does not necessarily flatten the curve, but it minimizes the overall infection through time. Such a reward could, for instance, potentially reinforce actions that lead to “steep” peaks instead of a flattened infection curve, as in practice it minimizes the area under the  $I(t)$  curve. Furthermore, as current containment controls may have effect if applied consistently and in the long term, such reward

<sup>3</sup><https://github.com/DLR-RM/stable-baselines3>

<sup>4</sup><https://github.com/thu-ml/tianshou>

<sup>5</sup><https://tianshou.readthedocs.io/en/latest/api/tianshou.policy.html?highlight=td3#tianshou.policy.TD3Policy>

design suffers from temporal credit assignment, since the reward value depends on a long and varying sequence of actions. Finally, any actions that happen after the peak infection occurrence will still be rewarded negatively, although such actions do not contribute to the goal minimization.

The next reward

$$\rho_2(t) = \begin{cases} 0 & , \text{if } t < T \\ -(\max_{t \leq T} \bar{I}_{G^*}(t))^2 & , \text{otherwise} \end{cases} \quad (21)$$

is designed to overcome the aforementioned shortcomings. This reward signal is sparse through time, as it is non-zero only at the last step of the control when the infection peak is known. The main property of interest of eq. (21) is that it has the same value as the loss that we used to train NODEC (see Equation (19)). This reward signal also suffers from credit assignment problems. As the reward is assigned at a fixed time and not as a direct result of the actions that caused it, the corresponding reward dynamics is non-Markovian [91]. To address challenges caused by rewards with non-Markovian properties, reward shaping[25] and recurrent value estimators [66] can be used. Furthermore,  $n$ -step methods or eligibility traces can be evaluated if we expect the reward signal to be Markovian but with long and/or varying time dependencies.

The final reward  $\rho_3(t)$  that we evaluated and used in the presented results is designed with two principles in mind:

$$\sum_t \rho_3(t) \approx \max_{t \leq T} (\bar{I}_{G^*}(t))^2 \quad (22a)$$

$$\arg \min_{t \leq T} \sum_t r_3(t) = \arg \max_{t \leq T} (\bar{I}_{G^*}(t)). \quad (22b)$$

Following those principles, the reward signal is approximately proportional to and provides information about the value of the infection peak used in the NODEC loss calculation. The reward sum minimizes exactly at the time when peak infection occurs. This property is expected to reduce effects of temporal credit assignment. When aiming to replace the proportionality in eq. (22a) with an equality, we reach the following reward signal design presented in the main paper eq. (18):

$$\rho_3(t) = \begin{cases} 0, & \text{if } \bar{I}_{G^*}(t) \leq \max_{\tau < t} (\bar{I}_{G^*}(\tau)) \\ -\bar{I}_{G^*}^2(t) + (\max_{\tau < t} \bar{I}_{G^*}(\tau))^2, & \text{otherwise} \end{cases} \quad (23)$$

It is straightforward to show that eq. (18) indeed satisfies  $\sum_t \rho_3(t) = \max_{t \leq T} (\bar{I}_{G^*}(t))^2$  and eq. (22b). This reward greatly improved performance without resorting to recurrent value estimators or further reward shaping. Still, after all proposed reward design and hyper-parameter optimization, NODEC has a higher performance (see fig. 10), although TD3 performs better than random control.

In figs. 6 and 8a the dynamic controls of both RL and NODEC seem to focus on protecting the target sub-graph by containing the infection as it spreads. In contrast to targeted constant control, they succeed in doing so by protecting driver nodes outside the target sub-graph. When comparing the dynamic control patterns, the budget allocation of NODEC seems to be much more concentrated on specific nodes, and it creates more often contiguous areas of containment.

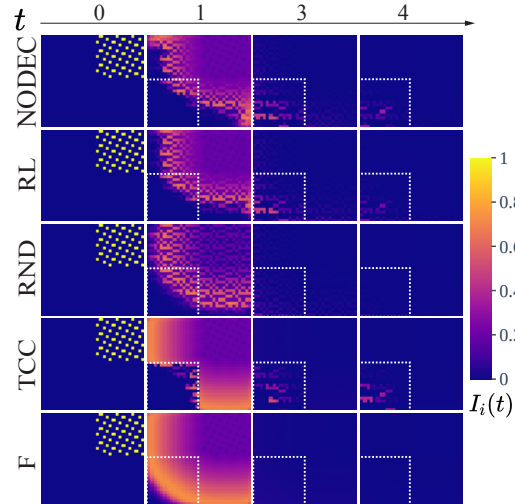
In fig. 10, we also show the evolution of  $S(t)$ ,  $R(t)$ , and  $X(t)$ . We observe that TCC and NODEC show clear signs of flattening the curve by preserving the highest susceptibility fraction and lowest recovery fraction at time  $T$ , which can be interpreted as less susceptible nodes becoming infected and needing to recover. The random method outperforms the other frameworks in terms of effective containment fractions, as random control assignments at each time step let the disease spread such that higher infection fractions  $I(t)$  are reached in the target sub-graph and therefore drivers with high infection fractions are effectively contained when controlled. Although low energy effective containment might seem favorable at first sight, it is not optimal in terms of flattening the curve with restricted budget, as it allows high infection fractions to occur within an area of interest. Budget restrictions often do not allow to fully constrain the spread in all infected nodes.

In fig. 9, we observe that although RL does not converge in terms of critic and actor loss, it still converges to a higher reward. This confirms that RL is capable of controlling continuous dynamics with arbitrary targets, but it requires significant parameterization and training effort to have good stable value estimates.

Finally, we tried to examine transfer learning capabilities from NODEC to RL. A closer look at fig. 4 reveals that the parameterized graph neural architecture used for NODEC and RL can be the same, i.e. there are no weights in the decision network layers of fig. 4. This means that the architectures trained with NODEC can be used as the “logit” action policy in RL, showcasing an effective use of transfer learning. In the given example, the RL policy network starting with trained NODEC parameters, is further trained for 100 episodes. After training, RL had a similar performance as NODEC since both methods flatten the curve at approximately  $\bar{I}_{G^*} = 0.0788$ . This means that RL did not improve the solution generated by NODEC. This example can be used to illustrate the interplay between NODEC and RL and how they can be used in synergy, e.g. when back-propagating through continuous dynamics is too expensive for high number of epochs. Reinforcement learning can be used as a meta-heuristic on top of NODEC, and the latter can be treated as an alternative to imitation learning.

Table 2: Tested and evaluated hyperparameters for the TD3 reinforcement learning baseline.

Hyper-Parameter	Value	Tested Values
Actor learning rate	0.0003	0.0003, 0.003, 0.03
Actor architecture	GNN	GNN, FC
Critics learning rate	0.0001	0.0001, 0.001, 0.01
Critics architecture	FC	FC
$\tau$ (Polyak update parameter)	0.005	0.005, 0.05
$\gamma$ (discount factor)	0.99	0.5, 0.8, 0.99, 1
exploration gaussian noise mean	0.01	0, 0.01, 0.1
update frequency of actor parameters	4 epochs	1–4 epochs
policy noise	0.001	0.001, 0.01, 0.1
noise clip	0.5	0.5, 0.2
reward normalization	True	True, False



(a) Infection spread on lattice for all baselines.

Figure 8: Infection spread from baselines.

## C Other Notes

### C.1 Hardware and code

Our experiments were mainly conducted on a dedicated server that was equipped with an NVIDIA TITAN RTX GPU, 64GB of RAM, and an Intel I9 8-core 9900KF processor. Partial code tests with assertions were conducted to examine (i) stiffness, (ii) numerical errors or bugs, and (iii) validity and similarity of the same dynamics controlled by different models. For the majority of the experiments seeds are fixed and initial states parameters

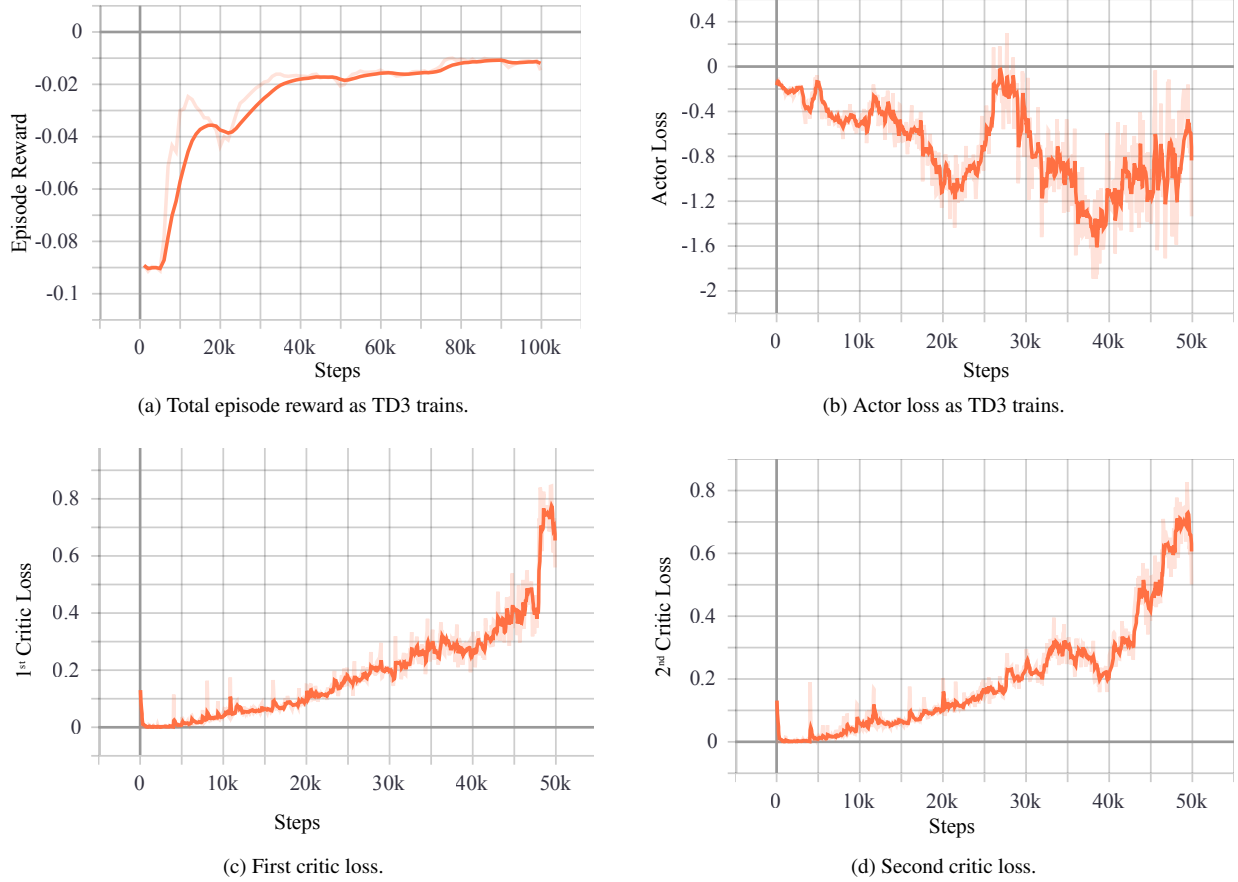


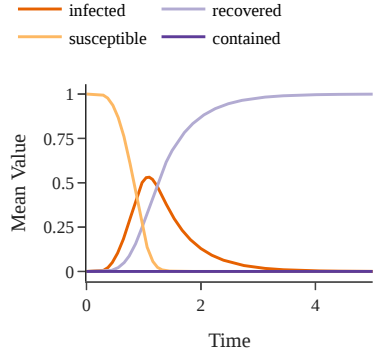
Figure 9: RL learning performance evaluation plots using Tensorboard using 0.8 smoothing.

are persisted in data files to enable reproducibility. ODEsolve and sample experiments may be affected by stochasticity on different machines. Based on statistical testing, we observe that with a good initialization and NN hyperparameter optimization, NODEC performs close to the reported values. Future works under provided repository, may perform extensive hyperparameter studies dedicated to specific dynamics, graphs. The average training time of NODEC per task is between 5-10 minutes depending on the complexity of the task. Baseline methods calculations and parameterizations would also take minutes, making time performance comparable.

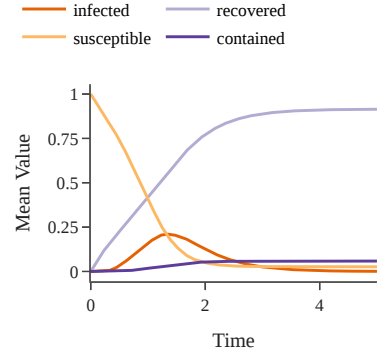
The project code can be found on GitHub <https://github.com/asikist/nnc> under MIT license. Numerical experiments are stored in the experiment folder (please check github README for more details).

## C.2 ODE Solvers and Stiffness

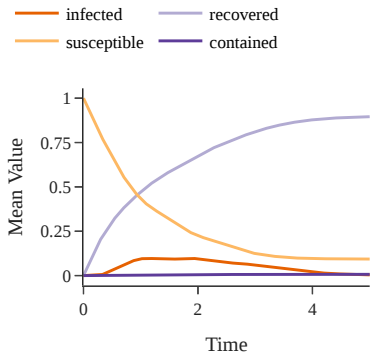
We prefer to use the Dormand–Prince solver [84] for the majority of our numerical experiments (in particular for training). For evaluating our results, we use a specific method, which allows the controller to change the control signal at constant time intervals. This choice allows us to compare control errors and energy costs without considering interaction frequency bias that occurs when one method outperforms another method because the solver allowed it to interact more often with the system and produce more tailored control signals. Adaptive step length allows the network to learn controls for variant interaction intervals and approximate continuous control better. We performed small-scale unit tests with VODE [84] against Dormand–Prince, Runge–Kutta, and implicit Adams implementations, and we noticed that for most



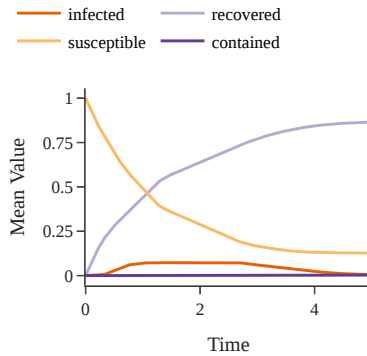
(a) SIRX curves for no control (F) baseline.



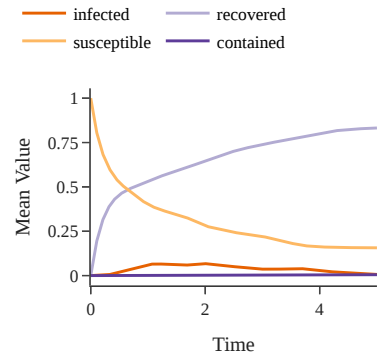
(b) SIRX curves for random control (RND) baseline.



(c) SIRX curves for reinforcement learning control (RL) baseline.



(d) SIRX curves for neural network control (NODEC) baseline.



(e) SIRX curves for targeted constant control (TCC) baseline.

Figure 10: SIRX curves for all baselines in the target subgraph  $G^*$ .

systems numerical errors were negligible.

The goal of this paper is to evaluate the ability of NODEC to learn controls within a solver. In future works that aim at controlling large-scale systems, different ODE solvers may be chosen according to the system's stiffness and performance requirements of the application. Whenever dynamics and training had high VRAM requirements, the adjoint method was used, mainly the implementations from Refs. [27, 49].

### C.3 Adaptive Learning Rate Training

Learning rate plays an important role on reaching a low energy control. In order to determine the optimal learning rate values we propose the adaptive learning rate scheme found in the Alg. 4.

---

**Algorithm 4:** Adaptive Learning rate training process of NODEC.

---

**Result:**  $\mathbf{w}$

```
1 Init:  $\mathbf{x}_0, \mathbf{w}, f(\cdot), \text{ODESolve}(\cdot), \text{Optimizer}(\cdot), J(\cdot), \mathbf{x}^*$ ;  
2 Params:  $\eta, \text{epochs}, \zeta, \text{tolRatio}$ ;  
3 epoch  $\leftarrow 0$ ;  
4 bestLoss  $\leftarrow \infty$ ;  
5 bestParams  $\leftarrow \text{copy}(\mathbf{w})$ ;  
6 previousLoss;  
7 while epoch < epochs do  
8    $t \leftarrow 0$  ;  
9    $\mathbf{x} \leftarrow \mathbf{x}_0$ ;  
10   $\mathbf{x}, \text{hasNumInstability} \leftarrow \text{ODESolve}(\mathbf{x}, 0, T, f, \hat{\mathbf{u}}(\mathbf{x}, t; \mathbf{w}))$ ;  
11  if  $J(\mathbf{x}, \mathbf{x}^*) > \text{tolRatio} \cdot \text{previousLoss} \vee \text{hasNumInstability}$   
12    then  
13    |  $\mathbf{w} \leftarrow \text{bestParams}$ ;  
14    |  $\eta \leftarrow \eta \zeta$ ;  
15    |  $\text{Optimizer.reset}()$ ;  
16    |  $\text{Optimizer.learningRate} \leftarrow \eta$ ;  
17  end  
18  else  
19    if  $J(\mathbf{x}, \mathbf{x}^*) < \text{bestLoss}$  then  
20    |  $\text{bestParams} \leftarrow \text{copy}(\mathbf{w})$ ;  
21    |  $\text{bestLoss} \leftarrow J(\mathbf{x}, \mathbf{x}^*)$ ;  
22    end  
23    previousLoss  $\leftarrow J(\mathbf{x}, \mathbf{x}^*)$ ;  
24     $\text{Optimizer.update}(\mathbf{w}, J(\mathbf{x}, \mathbf{x}^*))$ ;  
25  end
```

---